

Optimization of Excitation Waveforms for Maximum Instantaneous Field Intensity

Jakub Liska, Lukas Jelinek, Miloslav Capek, *Senior Member, IEEE*

Abstract—This paper introduces a computational approach to identify performance constraints in the time-domain based on optimizing the excitation waveform. The method builds on an optimization algorithm that has been employed for decades to establish fundamental limits in the frequency domain and this paper showcases its first comprehensive application to time-domain pulses. The method is applied to arbitrarily polarized multiport antennas and arrays. The demonstration performed is based on finding an antenna's maximum peak radiation intensity in a given direction and time with limited total input energy available. To highlight the generality of the approach, an analysis on finding optimal illumination for antiferromagnetic memory switching is conducted.

Index Terms—Optimal control, excitation, pulse radiation, peak power, electromagnetic radiation, antenna arrays, magnetic memories.

I. INTRODUCTION

SHORT electromagnetic (EM) pulse radiation is of significant importance in many fields, including applications involving impulse, short-pulse, or non-sinusoidal radars [1], [2], [3], ground penetrating radars [4] or through-wall imaging radars [5]. In addition to radar applications, an important discipline within the field is EM immunity testing [6]. Moreover, it has played a crucial role in communication systems that seek to increase information transmission rates [1], EM pulse applications, broadband arrays and high-energy directed beam systems [7], [8], [9], [10]. Apart from radioengineering, pulses are used across the whole spectrum of physics including antiferromagnetic switching which is analyzed in this manuscript.

Traditionally designed antennas using continuous wave analysis and synthesis techniques are frequently used to radiate short-duration pulses. Antennas with wide bandwidth are typically used, relying on the belief that they ensure sufficient performance. A more advanced approach involves matching an antenna excitation signal with its dispersion characteristics. Such an approach yields significantly better results [1], [11], [7]. There are no widely recognized standards for evaluating the performance of an antenna that radiates pulses, although the following are generally accepted: the pulse distortion in the radiation should be minor, the energy of the reflected signal at the input should be small, or the amplitude of the radiated pulse should be large [4].

Manuscript received January 3, 2025; revised January 3, 2025.

This work was supported by the Czech Science Foundation under project No. 24-11678S, and by the Grant Agency of the Czech Technical University in Prague under project No. SGS22/162/OHK3/3T/13.

J. Liska, L. Jelinek and M. Capek are with the Czech Technical University in Prague, Prague, Czech Republic (e-mails: {jakub.liska; lukas.jelinek; miloslav.capek}@fel.cvut.cz).

This paper establishes a computational approach to determine optimality in the radiation of directional pulses, generalizes the methodology, and allows the tool to be used in unconventional scenarios which had not been previously possible. The tool can assess the quality of an arbitrary antenna and give its optimal excitation.

An essential advantage of the proposed method lies in its ability to assess whether a given system configuration can achieve the desired pulsed performance. The method provides critical insights into whether optimization efforts can be confined to pulse shaping or whether a redesign of the system geometry is necessary. This dual capability offers valuable guidance for both waveform optimization and structural design, facilitating the decision-making process.

While co-design approaches that simultaneously optimize waveform and antenna design may approach globally optimal solutions, this work focuses specifically on waveform optimization for fixed antenna designs. By decoupling waveform optimization from antenna design, the method ensures broad applicability and low computational complexity.

To find the best possible excitation waveform, the optimization framework stems from the development of fundamental bounds on antenna performance in the frequency domain. By including commonly used computation methods, modern approaches, and evaluation techniques such as the electric field integral equation (EFIE) [12], method of moments (MoM) [13], convex optimization [14] and powerful computation units, limitations are often found on arbitrary quantities in various scenarios. A representative example is when efficiency, Q factor, and gain [15], [16] are intrinsically connected to directional pulse radiation which natively requires antennas with sufficient performance in these quantities. The method was initially introduced as antenna current optimization [17], and is based on current density being expressed in terms of EFIE and MoM representing degrees-of-freedom (d-o-f) in convex optimization. In state of the art in fundamental bounds in electromagnetism [18], quantity trade-offs [15], [19], tighter bounds including additional constraints [19], or quantities in specific scenarios, such as implanted antennas [20], are evaluated. The phenomenon is also well developed in fields unrelated to antennas, *i.e.*, cloaking [21], heat transfer [22], magnetic trapping [23], and harmonic generation [24].

A few works addressing optimal excitation in the time domain have been done, notably those considering radiated pulse optimization in [8], [25], where up-to-date methodologies are not used. Initial attempts to use modern tools in the optimization of radiated pulses are presented in [26]. The results show optimality in peak radiation intensity in a given direction of

linearly polarized dipole-type antennas, such as the dipole, bowtie, and exponentially tapered bowtie. Evaluation consists of a large number of frequency samples computed using EFIE and MoM to optimize the excitation using the quadratically constrained quadratic program (QCQP) [14], [27] in the frequency domain and then mapping by inverse fast Fourier transform (iFFT) to the time domain [26]. The extension of the method to arbitrarily polarized antennas was initialized in [28].

In this paper, in addition to the applicability of the approach to an almost arbitrary problem using any simulation software, multiport antennas and arrays are the novel features described, as discussed in Section IV. The section III presents the framework in detail and follows the flow chart in Fig. 1 where individual steps are given. Most steps are performed using well-developed, proven techniques in the frequency domain for antenna analysis and computation of fundamental bound. The procedure allows for direct control of the frequency range of the optimal excitation pulse which is always band limited, *i.e.*, angular velocity $\omega = 2\pi f$ and frequency f are considered from f_{\min} to f_{\max} , given by realistic values¹ for pulse generators.

The remainder of the paper is organized as follows. Section II describes the history of how to generate excitation for optimal pulses. The established computation framework for optimal directionally radiated pulses is presented, tested, and verified in an example in Section III, whereby a comparison of the performance of different antenna designs allows the best one to be chosen, and assists in deciding on the optimal layout of an array for pulsed radiation. Using the same methodology, the optimal illumination for antiferromagnetic memory switching is found in Section IV. Capabilities, limitations, and possible extensions are discussed in Section V.

Although this work primarily focuses on optimizing excitation waveforms to achieve power metrics in far-field scenarios. The proposed framework is easily adjustable for near-field energy focusing or similar applications where precise waveform shaping is crucial, given the knowledge of the impulse response in the respective region. However, this work does not address the practical aspects of designing pulsed systems but instead provides a versatile theoretical methodology that is applicable in diverse contexts.

II. HISTORICAL BACKGROUND

This section recalls work done on optimal pulsed radiation, an oft-ignored topic in recent times, and highlights the novelty provided within this paper.

The critical advancement to uncovering the optimality of antenna pulse radiation lay in using an excitation signal precisely tailored to the specific dispersion characteristics of the antenna [1]. Achieving this would result in a flat frequency response producing the highest possible pulse amplitude and maximizing the strength of the electric field at a given moment and point in the far field. For arbitrarily shaped antennas, with

¹For instance, regarding antenna radiation, the frequency band is constrained using step-recovery diodes [29] with $f_{\min} = 0$ Hz and $f_{\max} = 3.8$ GHz.

a particular emphasis on planar pulse radiators, the search for optimality is detailed in [1] and provides insight into performance maximization related to size and bandwidth. The methodology assumes an arbitrary planar current distribution confined to the design region. Although this understanding of bounds provides valuable insight, it falls short of synthesizing practical and applicable designs.

In [7], a distinct performance maximum of pulse radiation is initially introduced to examine the optimal input voltage. The metric and computational approach studied remain consistent. This exploits the computation in the frequency domain, using iFFT, and applies variational optimization to maximize the amplitude of the radiated electric field at a specified time and position in the far field with constrained energy² and the bandwidth of the applied signal. Compared to [1], the current in [7] is physically realizable bringing this solution closer to practical implementation as long as the feed voltage can be generated or sufficiently approximated. Although the solution in [7] refers to a dipole antenna, it accommodates arbitrary feed point locations, lengths, or impedance loadings. In these works, the current distribution is determined using EFIE and the Galerkin method to employ piecewise sinusoidal expansion [30].

The progression of the study in determining the optimal transient radiation of arbitrary antennas is documented in [8], [31] and extends the analysis to three-dimensional antennas compared to planar radiators in [1]. The objective metric remains the same as before. Furthermore, the study addresses the maximum possible radiated energy density within a specified time interval while considering the effects of introducing constraints on the sidelobes. Physical realizability is emphasized by limiting Q or super-directivity effects. Fundamental limitations are juxtaposed with the performance of optimally fed antennas [7], [31] and dipole arrays [9], all of the same size [8], [31]. This work builds on [32] and employs spherical mode expansion. Limiting the number of spherical mode expansion terms ensures a low antenna Q and mitigates impractical supergain issues. The Chebyshev synthesis procedure is used to constrain the energy radiated in the side lobes.

Supplementary to [7] and in alignment with [8], optimal excitations for dipole arrays aimed at maximizing the amplitude of the transient radiated electric field at a specified time and position in the far field are detailed in [9], and maximizing energy density in a given time interval at a fixed far-field position are detailed in [2]. As with [7], the MoM is employed to calculate the currents on all dipoles, taking into account the effects of mutual coupling. Piecewise sinusoidal expansion modes are used, reflecting the approach in [7]. The relationship between the total radiated field and terminal voltages is established by superposing the far fields of each terminal. This analysis uses a thin-wire approximation for the dipoles and delta gaps to model their feed-voltage sources. The d.o.f in this study encompass the magnitudes and phases of the terminal voltages. Furthermore, the investigation is extended to the synthesis of optimal sidelobe patterns.

²Constraining the root mean square current amplitude over the surface of the radiator was implemented in [1], [7].

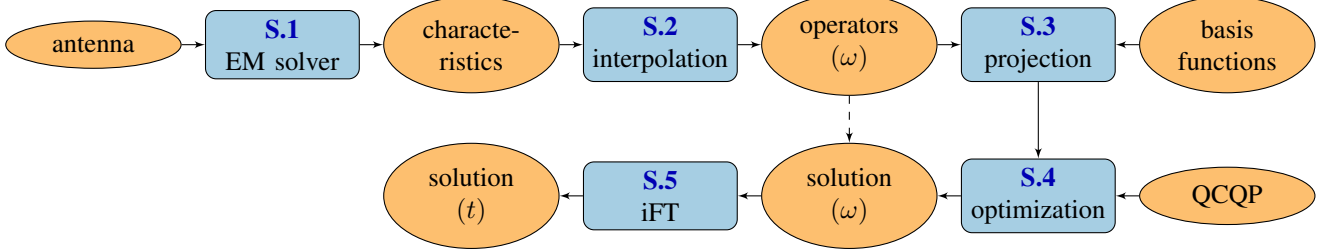


Fig. 1. Flow chart of the computation steps **S.1** – **S.5**, starting from the given antenna and port with the characteristic impedance of the feed transmission line and finishing with the optimal solution in the time domain, *i.e.*, the optimal excitation and performance value.

Alternatively, one might consider whether the radiated electric field at a far zone is equal to a predetermined function of time rather than focusing on maximizing field intensity. This question is addressed in [10]. In specific applications, such a criterion may be more suitable than maximizing the radiated field amplitude or energy density at a particular time and position in the far zone. The solution to this problem is carried out entirely in the time domain by minimizing a particular norm of the difference between the required and actual electric fields at a point lying in the far zone. The paper tackles the inverse source problem, specifically constructing the input voltage for a given far-zone electric field function of time via an iterative optimization algorithm based on the steepest descent.

In addition to finding optimal antenna excitation, there is a search for optimal antenna design with regard to pulse radiation which cannot be accomplished using conventional antenna synthesis techniques [1]. This question is explored in [4] with a focus on the optimality of conical antennas and in [33] with an emphasis on bowtie antennas. The theoretical analysis used to optimize the conical antenna is grounded in the time domain. Geometrical parameters and resistive loading are adjusted to maximize radiated energy for a given excitation. Similarly, dipole shapes are optimized [34] using the conjugate gradient method.

Given that all previous work has focused on radiation in the far-field zone, the study of the near-field zone remains open. Concentrating EM energy in small regions for short intervals has emerging applications in biomedical applications, such as hyperthermia therapy to treat cancer and other diseases [3]. The approach to achieve a high concentration of EM energy in small regions involving free space and non-dispersive materials is presented in [3]. The framework is demonstrated with linear arrays. Intuitively, the timing of the sources must be adjusted to compensate for differences in the propagation path lengths so that transmitted pulses from the array elements are coherently added at the target location.

Moving to communication systems, optimizing the transient waveform should consider both the transmitting and receiving antennas, in contrast to the work mentioned above. In ultra-wideband (UWB) radio systems, the crucial metric is the maximum amplitude of the received antenna voltage, its sharpness, or energy, as addressed in [35]. Unbeatable target metrics are achieved by finding the best-performing waveform considering the constraints on energy in different stages of the channel.

General optimization results are derived for arbitrary antennas, considering the effects of the generator and load impedances using variational methods. The approach is demonstrated with dipoles using MoM³ solutions providing the necessary transfer functions and input impedances from the EFIE analysis with the study enriched by closed-form results for short-dipole antennas. Ideally, an UWB transmitter's radiated power spectral density should be as flat as possible. However, in reality, UWB systems are limited by the performance of the antennas which is far from ideal [35].

The precise metric for the sharpness of the received antenna voltage amplitude and its optimization are detailed in [36]. The objective is the maximal derivative of the receiving voltage waveform. A substantial improvement is observed compared to [35] with results validated through measurement.

III. FRAMEWORK

This section develops and verifies the general computational approach for optimal excitation and showcases it on particular example of pulsed radiation in a chosen far-field direction and time. Various goals and objective functions with multiple constraints can be considered within the approach presented in this article. The essential user input for the computation is the relation between the excitation and the target metric, *i.e.*, a solution to Maxwell's equations. Knowing the system response, almost arbitrary linear scenarios can be studied, including optimization of radiated field intensity, power delivery efficiency, or waveform shaping tailored to specific spatial or temporal requirements. This versatility makes the framework applicable to scenarios such as pulse radiation enhancement and electromagnetic field focusing in localized regions. In addition to the examples given in the manuscript, notable applications might be the wireless power delivery from the port of an antenna to the port of another antenna and the creation of hot spots in the near field. The practical usage of the method is given in Section IV where several applications are considered.

A. Methodology

A representative goal used to demonstrate the methodology, which is widely analyzed in this manuscript, is to find an antenna's maximum peak radiated power in a given direction and time with limited available total input energy available.

³Piecewise sinusoidal basis is used as well, as in [7], [9].

Mathematically speaking, the problem reads,

$$\begin{aligned} & \max_{\mathbf{a}(t)} r^2 \mathbf{r}_0 \cdot \mathbf{S}(\mathbf{r}, t_0 + r/c), \\ & \text{s.t. } W_{\text{inc}} = W_0, \\ & f \in [f_{\min}, f_{\max}], \end{aligned} \quad (1)$$

where

$$\mathbf{r}_0 \cdot \mathbf{S}(\mathbf{r}, t) = \frac{1}{Z_0} |\mathbf{E}_\infty(\mathbf{r}, t)|^2. \quad (2)$$

The incident waves $\mathbf{a}(t)$ on the feeding transmission line connected to the antenna ports are optimized to maximize radial component \mathbf{r}_0 of Poynting vector \mathbf{S} at given point \mathbf{r} and time $t_0 + r/c$ which is normalized by the squared distance from source r^2 . For convenience, the observation time is shifted by the free-space propagation delay caused by the speed of light c . Impedance Z_0 in (2) denotes the impedance of the free space and \mathbf{E}_∞ denotes the electric intensity in the far-field region. Total incident wave energy W_{inc} is set to be total available energy W_0 . This work considers 50-Ohm feeding transmission lines and energy $W_0 = 10^{-10}$ J.

The solution to such a problem can be achieved by taking the following steps:

S.1 First, an antenna with defined ports and feeding transmission lines has to be chosen. The setup is analyzed in an arbitrary electromagnetic (EM) solver, which can compute the far field in the desired direction for a given frequency and incident waves on the feed lines to the antenna ports. The EM solver provides a set of far-field values. An arbitrary method, capable of evaluating target quantities for a given excitation, can be used, *i.e.*, finite differences in time domain (FDTD) in CST studio suite [37] (CST). This part of the process is computationally the most time-consuming. The computational demands grow with wider frequency ranges $f \in [f_{\min}, f_{\max}]$, but these, on the other hand, introduce more d-o-f in the waveform design providing greater flexibility in shaping the radiated pulses.

The electric field in the far-field zone expressed in the frequency domain reads

$$\mathbf{E}_\infty(\mathbf{r}, \omega) = \mathbf{H}(\mathbf{r}, \omega) \mathbf{a}(\omega) e^{-j\omega r/c}, \quad (3)$$

where \mathbf{H} is a far-field transfer matrix obtained from the chosen solver and $a(\omega)$ represents incident waves in the frequency domain (for example, power waves in the feeding transmission lines), *i.e.*, Fourier transform of $a(t)$. An example of getting the transfer matrix is the combination of the EFIE and the MoM detailed in Appendix A. Apart from the quantities needed for optimization, antenna properties such as the reflection coefficient or gain at given frequencies can be examined to provide insight into the spectral selectivity of the antenna.

S.2 The far-field data are interpolated using rational fitting (sparse data) or linear interpolation (dense data) to provide a smooth function of frequency. In this step, the operator for total incident energy is prepared, namely the identity operator in the quadratic form of the incident

waves meaning the incident energy is written as a spectral integral

$$W_{\text{inc}} = \frac{1}{4\pi} \int_{-\infty}^{\infty} \mathbf{a}^H(\omega) \mathbf{a}(\omega) d\omega. \quad (4)$$

S.3 The spectral functions representing the necessary operators for optimization, *i.e.*, total incident energy, and the far field are projected onto a set of continuous-band-limited basis functions. The projection follows Galerkin method [38], [13]. The set of basis functions $\xi_n(\omega)$ is described in Appendix B. For all considered examples, number of basis functions⁴ $N \leq 120$ was sufficient. The projection results in expansion coefficients of the basis function grouped in column vector \mathbf{q} , where

$$a_p(\omega) = \sum_n q_{pn} \xi_n(\omega). \quad (5)$$

The vector is constructed in segments with each segment comprising the expansion coefficients of the basis functions for each feed line p . Related matrices \mathbf{W}

$$W_{\text{inc}} = \mathbf{q}^H \mathbf{W} \mathbf{q} \quad (6)$$

(incident energy) and \mathbf{S} (far-field power) are derived via Galerkin method from (4) and (2) together with (3), respectively.

As an example, the incident energy (4) is represented by matrix \mathbf{W} , the components of which read

$$W_{pm,qn} = \frac{\delta_{pq}}{4\pi} \int_{-\infty}^{\infty} \xi_m^*(\omega) \xi_n(\omega) d\omega, \quad (7)$$

where pm, qn corresponds to the matrix rows and columns according to feeding lines p, q and basis function m, n , respectively. Kronecker delta δ_{pq} is zero except when p and q refer to the same port. Since the ports are separated and the basis functions are orthogonal to each other with respect to the given integral, the identity matrix represents the total incident energy matrix \mathbf{W} . Equivalently projection of other operators considered in this methodological example are presented in Appendix C.

S.4 The expansion coefficients are optimized to maximize peak radiated power at the given time and direction according to (1) and the equivalent QCQP reads

$$\begin{aligned} & \max_{\mathbf{q}} \mathbf{q}^H \mathbf{S} \mathbf{q}, \\ & \text{s.t. } \mathbf{q}^H \mathbf{W} \mathbf{q} = W_0. \end{aligned} \quad (8)$$

The optimization task is resolved using standard methods of the QCQP. The optimization problem is convex, so the solution is unique [14], which ensures that the maximum is truly achieved⁵. Within this paper, the optimization is more than a thousand times faster than the computation

⁴Later, the number of basis functions is the number of d-o-f in the optimization and determines the time needed for construction $\mathcal{O}(N^2)$ of matrices and solution $\mathcal{O}(N^3)$.

⁵The optimization problem is equivalent to that for determining performance limitations on antenna metrics in the frequency domain [19].

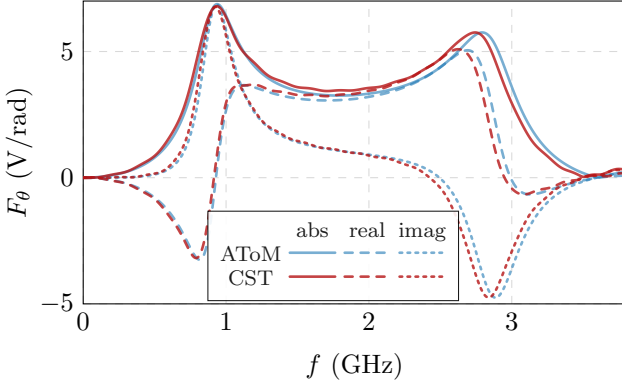


Fig. 2. Far field of a dipole antenna with a length of 15 mm and width of 3 mm in directions $\varphi = 0$ and $\theta = \pi/2$. The antenna is fed through a delta-gap source connected to the feed line, providing a voltage of 1 V across the entire frequency spectrum.

of the impulse response of the system. For more details about the convex optimization framework, see [39].

S.5 The solution is found as optimal vector \mathbf{q} in the frequency domain. The linear combination on the feed line then gives the optimal feeding vector which results in maximum peak radiated intensity in the frequency domain using the operators of step **S.2**.

The solution is transformed to the time domain via inverse Fourier transform (iFT) either as a single function or by weighted summation images of the basis functions $\xi_n(t)$. The far field is also transformed to depict the radiated pulse waveform in the time domain.

Although described for far-field radiation scenarios, the methodology explained above is general and can easily be applied to different directions and extended to applications such as near-field energy focusing, wireless power transfer, or UWB radars. However, we intentionally omit design concerns related to these systems, such as topology optimization of the radiating and receiving antennas. We focus solely on feeding waveform optimization, which is, unlike topology optimization, a convex optimization problem.

B. Verification

The steps mentioned above are applied to an example of a single dipole antenna. The calculation is simultaneously performed in the Antenna Toolbox for MATLAB [40] (AToM) and CST. The dipole with a length of 15 mm and a width of 3 mm is oriented along the z axis. The port is placed in the middle of the dipole and is connected to an ideal 50Ω feed line. Radiation in the spherical coordinate system is studied in the direction $\varphi = 0$ and $\theta = \pi/2$. Azimuthal coordinate φ references to angle from positive direction of x axis in xy plane and elevation coordinate θ references to angle from positive direction of z axis.

The antenna, including the port, is given, and all steps visualized in Fig. 1 can be performed. Choosing AToM and CST as the EM solvers and computing the far-field component F_θ in elevation direction for unity excitation at all frequencies results in Fig. 2. Since the dipole is aligned along the z -

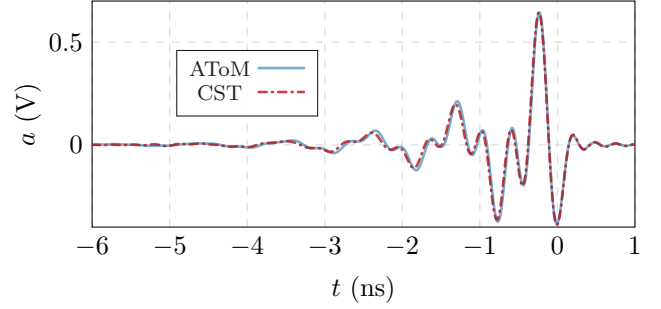


Fig. 3. Optimal waveform of the incident wave gained from analysis in different solvers. In both cases of AToM and CST, optimization is performed in MATLAB.

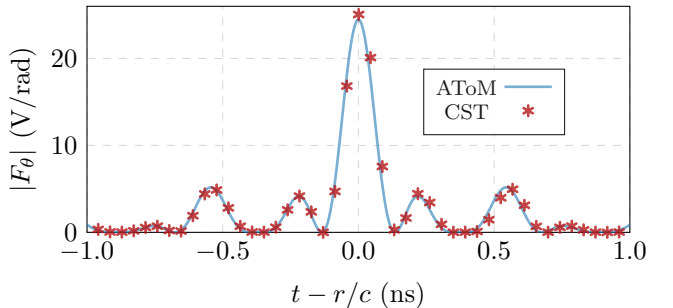


Fig. 4. Optimal radiated waveform for $t_0 = 0$ s at distance r gained from iFT of the far field for AToM data and monitoring the far field during simulation in CST, where the optimal incident wave is applied as excitation.

axis, only the θ component of the electric field corresponds to radiation. The curves are in good agreement.

In addition to the far field, an essential known characteristic is total incident energy, represented by the identity operator as seen in (4). This step accomplishes **S.1**.

Since the frequency data from CST are dense due to the 1001 samples, only linear interpolation is used. Data resulting from AToM are sparse and rational fitting is used for interpolation⁶.

Metrics such as far field and total input power are projected to the band-limited functions defined in Appendix B resulting in matrices as denoted in **S.3**. The matrix operators allow for optimization **S.4** which gives the optimal solution in the frequency domain.

Since the basis functions used for projection are orthogonal and an identity operator represents total input power, the matrix for total input power is an identity matrix. The optimal excitation is a complex conjugate of the far field [1] in Fig. 2. Total input energy is $W_0 = 10^{-10}$ J. Meeting the constraint in (8) is ensured by scaling the magnitude of the incident wave. The optimal waveform in the time domain is the result of iFT in **S.5**, and is plotted in Fig. 3. The agreement of different solvers is more than satisfactory.

The last step is the computation of the radiated pulse, shown in Fig. 4. The similarity of the data computed by AToM with iFT and a synthetic measurement of the radiated pulse by optimal waveform excitation in CST verifies and, even more,

⁶Vector fitting [41] could be applied to enforce passivity and causality.

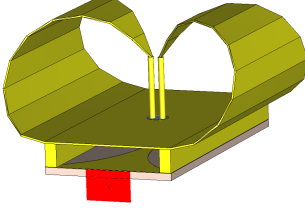


Fig. 5. Self-grounded bowtie antenna with matching circuit as described in [42].

generalizes the method for determining optimal pulses studied for decades [7], [9], [31], [26], [28]. In addition, this framework allows us to find an optimal excitation using an arbitrary solver and do it for complex scenarios, as demonstrated in the following section.

IV. REPRESENTATIVE EXAMPLES

Multiple antennas and arrays are analyzed using the presented approach. Moreover, this section extends the study to antiferromagnetic memory switching where the target is the electric field magnitude at a chosen point excited by a pulsed incident field. Additional research is also conducted on the energy delivered to the given point during the chosen time interval. Since the solution is independent of the solver, as verified in the previous section, the most suitable one can be used for each scenario.

A. Far-Field Pulsed Radiation

1) *Singleport Antennas*: As has been concluded in previous work, the bowtie dipole antenna exhibits good performance among planar antennas studied for pulsed radiation in the direction orthogonal to the design plane [26], [28].

In this section, the following antennas are considered: a self-grounded bowtie antenna, a conical dipole antenna, a conical spiral antenna, and a logarithmic periodic antenna. The optimal waveform is determined to maximize the radiated peak power. None of the antennas are topologically optimized for the target. This example aims to demonstrate the utility of the approach and compare the best potentially achievable performance of the proposed antennas, including their optimal excitation waveform.

All samples can be circumscribed by the smallest sphere with a radius of $a = 36$ mm. The allowed frequency band of the input signal is chosen between 0 GHz – 15 GHz. The antennas are simulated as if made of copper and connected to the 50Ω feeding line. The observation point of the pulse radiation is always chosen in a direction native to each antenna.

The self-grounded bowtie is taken as proposed in [42], the model is created and simulated in CST and can be found in Fig. 5. The authors ascribe great performance in pulsed radiation to this format.

A planar version of the bowtie antenna is analyzed in [26], [28] in relation to pulsed radiation. To take advantage of the volume of the circumscribed sphere, a volumetric bowtie dipole antenna is considered and scaled to fit the sphere. See

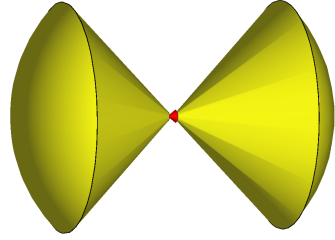


Fig. 6. Volumetric bowtie dipole antenna.

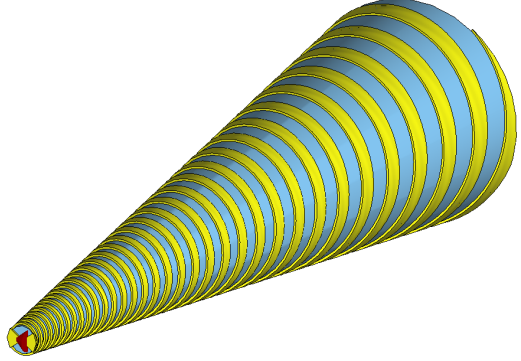


Fig. 7. Conical spiral antenna for ground penetrating radar [43].

Fig. 6, which is taken from CST, where the simulation is performed.

In [43], the conical spiral antenna is proposed for ground-penetrating radars, an UWB application. The conical spiral radiates a circularly polarized field compared to the other designs which operate in a linearly polarized regime. The antenna proposed in [43] is scaled to fit the circumscribing sphere mentioned above. The simulation is again performed in CST and shown in Fig. 7.

The periodic logarithmic antenna, recognized as an UWB antenna [44], is extensively utilized in electromagnetic emission and immunity testing [6]. Therefore, a wire dipole array is a potential candidate for pulsed radiation and is compared with other antennas. The array is designed to fit the circumscribing sphere and exhibits a decay of 0.9 in element lengths and an opening angle of 15 degrees. The strip width equals 0.017 times the length of the longest element and the number of elements is 20. The antenna is simulated using AToM and shown in Fig. 8.

The question remains as to which antenna performs better. A comparison is shown in Fig. 9. The logarithmic periodic antenna exceeds the other designs in performance. The performance of the self-grounded bowtie antenna is about two times lower and the other designs perform even worse. This finding could prompt efforts to develop improved designs.

Regarding the origins of what constitutes good performance, the realized gain in the given direction accounts for the pulse's sharpness and energy. The emerging differences of the antennas are depicted in Fig. 10 which justifies the performance differences presented in Fig. 9. The highest and flattest realized gain gives the best performance which provides some direction for improved future designs.

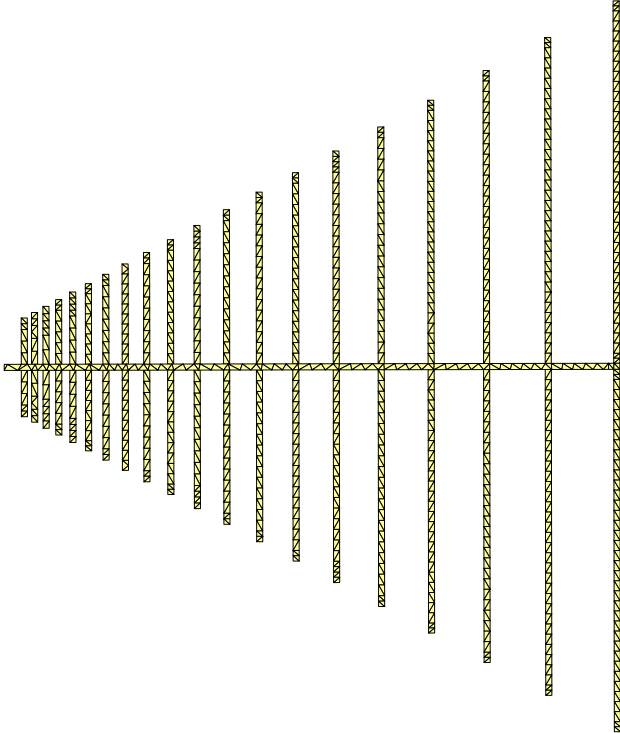


Fig. 8. Logarithmic-periodic dipole wire antenna designed according to [44]. The antenna is discretized in the mesh of 1528 triangles.

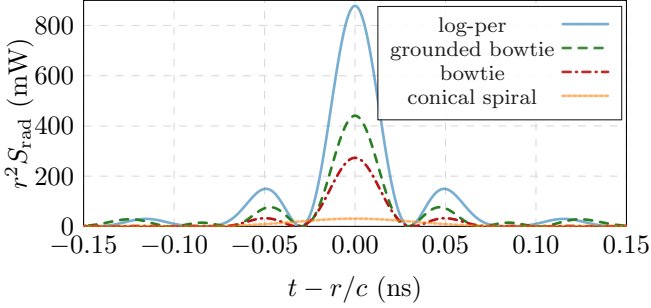


Fig. 9. Normalized optimal radiated pointing vector at chosen distance r of the compared antennas.

In contrast, phase properties must be considered once an optimal excitation signal is generated. Abrupt changes in phase require more complex excitation than antennas with linear phase progress which prefer short excitation waveforms. The optimal excitation waveforms shown in Fig. 11 illustrate the ability of the approach to determine the optimal excitation for an arbitrary setup and how realistic it is to achieve the best performance of the given antennas.

The significant difference in excitation signals is visible for the bowtie and periodic antennas. Sharp excitation is preferred by bowtie antennas as compared to periodic antennas which require a longer waveform for pulsed radiation. The delay in the antennas is also noteworthy as the bowtie antenna immediately radiates energy, whereas the grounded bowtie excitation signal shows a delay in the matching circuit. Meanwhile, the periodic antennas, namely the logarithmic and conical spiral ones, accumulate energy first.

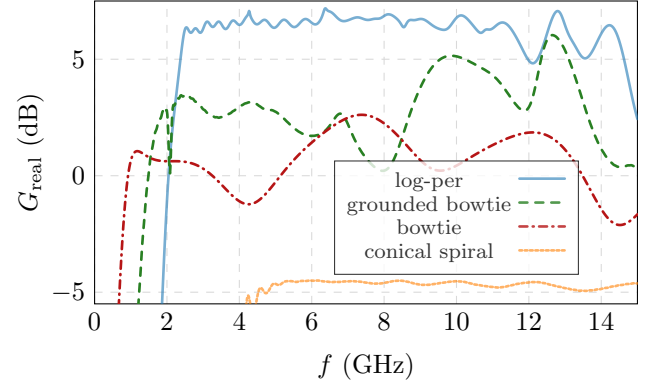


Fig. 10. The realized gain of the antenna, which incorporates both the antenna gain and the effects of impedance matching, is a critical factor for achieving optimal performance.

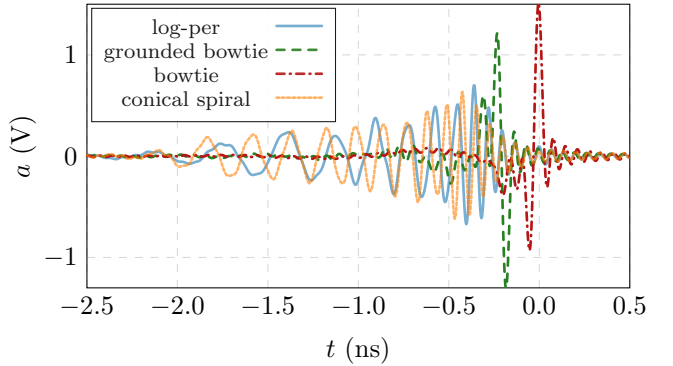


Fig. 11. Optimal excitation signals achieving the highest performance in pulsed radiation for individual antennas.

The comparison of the antennas and the finding of the optimal excitation using the approach proposed in this paper show that antenna design and pulse generation capabilities are closely related. The information that can be provided by this computational approach can provide essential insight into designing antennas that perform well in pulsed radiation.

Notably, within the optimization framework (1), constraints on field intensity at spatial points can be included without compromising generality or convexity. Similarly, upcoming sections demonstrate the imposition of energy constraints at the target point within a time window. This method can also be extended to additional spatial points outside the main direction and time frames, still using the same framework. However, the inclusion of these constraints may result in an increase in the duration of the optimization process.

2) *Multiport Systems*: The extension to multiport antennas or arrays is straightforward, as with dipole arrays within this section. The matrix formulation is also shown in (7), Appendices A and C.

The goal of this section is to show whether end-fire or broad-side pulsed radiation perform better in the setup of the four active dipoles discussed in Section III. The dipoles are spaced half a wavelength at 1 GHz. Again, a band limited from above by frequency 3.8 GHz is considered.

The optimal radiated pulses of all configurations are com-

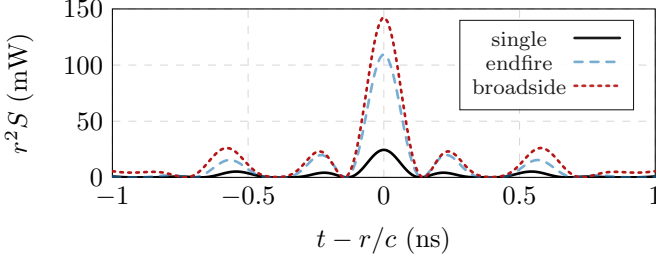


Fig. 12. Normalized Poynting vector of a single dipole antenna and array radiated in the end-fire and broadside direction.

pared in Fig. 12 where the magnitudes of the radiated Poynting vector peaks S are given and normalized by radial distance r . The results show that broadside radiation performs better than end-fire.

Considering the same input energy, the end-fire array increases the performance by more than a factor of four as compared to a single dipole. In the case of a broadside array, the performance boost reaches a factor of six. The difference may be due to the coupling of the field with the elements of the arrays which can be deduced from the optimal excitation waveforms in Fig. 13. Although the end-fire and broadside arrays share the same configuration, their characteristics, especially impedance ratios, differ since the dipoles are fed simultaneously. In this particular case, the broadside direction performs better than the end-fire orientation.

The excitations to all ports are almost identical in broadside operation. For the end-fire array, the delay equal to the distance between the dipoles multiplied by the speed of light is observed. The delays agree with the direction of end-fire radiation which points from dipole port 1 to dipole port 4. The magnitude of the excitation pulse is increased from dipole port 1 to dipole ports 2, 3, and 4, which indicates that the last element contributes the most.

The suggested approach can be applied to multi-dimensional arrays or any radiating structures with multiple ports and arbitrary configurations. Typically, computational demands grow as the number of elements increases. As demonstrated, expanding the number of independent ports results in expressing the excitation waveforms at each port through the basis functions described in Appendix B. The expansion coefficients are distinctively grouped into a vector that includes all d-o-f.

B. Switching Antiferromagnetic Memory

The approach mentioned in this manuscript can be generalized in an arbitrary application where the input-output relation is known. In this section, the switching of an antiferromagnetic memory using a device illuminated by a pulsed laser is analyzed. The data are taken from [45]. The goal is to reach a peak electric field intensity high enough for memory switching.

The device is electrically large so the full simulation is computationally expensive. The experimental illuminating field is a Gaussian beam from a parabolic mirror with a diameter comparable to the cross-section of the device. However, the simulation in CST is done only for the central part of the device, as seen in Fig. 14, and the plane wave is considered

as excitation. Due to the large width of the beam as compared to the target, the plane wave is an excellent approximation and simplifies the calculation. Compared to the original geometry [45] the motive is made three times smaller. This shifts the frequency behavior to higher bands and results in improved performance of the excitation used.

The metric of interest is electric field intensity in CuMnAs layer E_{CuMnAs} in the center of the motive shown in Fig. 14. The CuMnAs motive is prepared on a GaAs substrate and most of the CuMnAs alloy is covered by Au, except the central part as described in [45]. Incident field E_{inc} is the excitation, which is represented by plane wave propagation orthogonally toward the motive, and polarization is aligned with two of the electrodes. The delay from the source to the point of observation in CuMnAs is estimated to be 0.2 ps.

The excitation waveforms are plotted in Fig. 15. The pulses are normalized to the maximum value of 10^5 V/cm. The excited field magnitude in CuMnAs is provided in Fig. 16.

The pulse used in [45] is denoted as (o). Using the optimization framework within this paper, maximum switching performance is determined. The objective function is the magnitude of the electric field intensity in CuMnAs. The excitation is limited in frequency from 625 GHz to 2.8 THz. The constraint on the frequency band pertains to the frequency range of the excitation pulse (o). Incident field energy is limited and excitation pulses are normalized to have a maximum amplitude of 10^5 V/cm as in [45].

One of the optimal pulses presented corresponds to the maximum magnitude of the electric field in CuMnAs in $t = 0$ which is denoted as (a). The optimization problem is identical to (8) other than matrix \mathbf{S} being replaced by $\mathbf{E}^H \mathbf{E}$, where the electric field at the target point is represented as $\mathbf{E}_{\text{CuMnAs}}(\omega) = \mathbf{E}(\omega) \mathbf{q}$ in the frequency domain, and \mathbf{q} corresponds to the expansion of incident plan wave $a(\omega)$ into the basis functions of Appendix B, as done in (5). The relation is computed using CST which allows us to compute the electric field at a given point as a function of frequency considering unity excitation. Mapping the set of the given basis functions results in the desired matrix. The matrix representing the total energy of the incident plane wave is derived from (4) as demonstrated in (7), with the only variation being the inclusion of the free space impedance in the denominator.

The maximum amplitude of the electric field in the CuMnAs alloy significantly exceeds that of the pulse used (o). However, the excitation pulse has a long duration and is quite complex compared to (o). Moreover, the resulting electric field in CuMnAs has many peaks and a long duration.

This evidence indicates the necessity of introducing constraints on the input and output waveforms. The incident wave is constrained to have 90 % energy in the interval $[-1.2, 0.8]$ ps taking into account the delay of $t_d = 0.2$ ps. The constraint is implemented using matrix \mathbf{W}_T of total available energy and

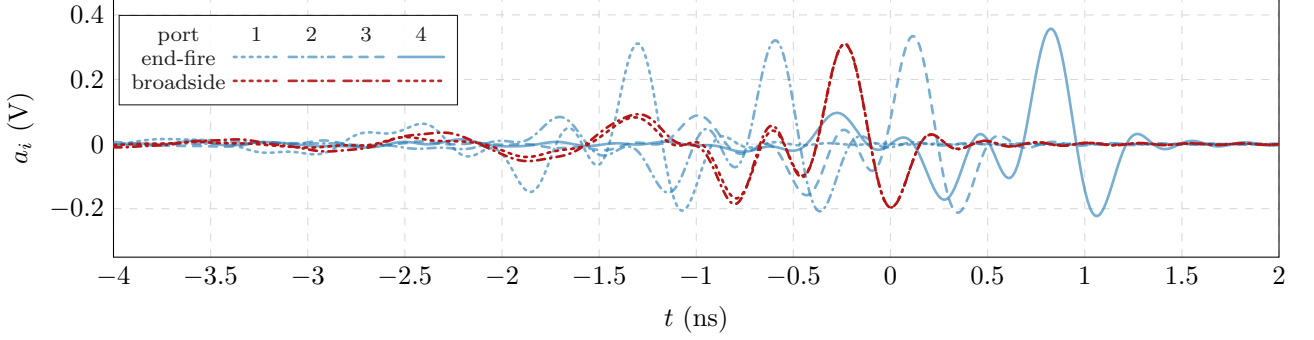


Fig. 13. Optimal excitation signals for end-fire and broadside pulsed radiation.

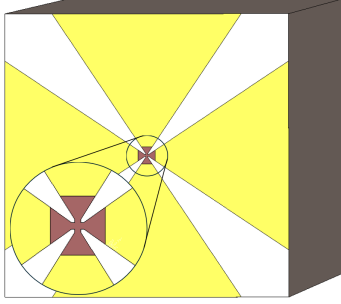


Fig. 14. CST model of the central part of the antiferromagnetic memory [45] with zoomed target middle section.

energy available in the interval [2]

$$W_T = \frac{1}{4\pi^2 Z_0} \int_{-\infty}^{\infty} \int_{-\infty}^{\infty} \frac{2 \sin [(\omega_1 - \omega_2) T]}{\omega_1 - \omega_2} e^{-j(\omega_1 - \omega_2)t_d} a^*(\omega_2) a(\omega_1) d\omega_2 d\omega_1, \quad (9)$$

where $T = 1\text{ ps}$ is the half-time interval and the asterisk represents a complex conjugation. In the frequency domain, the sinc function represents the process of time windowing. The matrix obtained is the outcome of the procedure illustrated in (7) regarding total input power. The corresponding QCQP reads

$$\begin{aligned} & \max_{\mathbf{q}} \mathbf{q}^H \mathbf{E}^H \mathbf{E} \mathbf{q}, \\ & \text{s.t. } \mathbf{q}^H \mathbf{W} \mathbf{q} = W_0, \\ & \quad \mathbf{q}^H (0.9 \mathbf{W} - \mathbf{W}_T) \mathbf{q} \leq 0. \end{aligned} \quad (10)$$

The optimization solution is denoted as (b). The incident field waveform is now squeezed in the given narrow interval and is similar to the original pulse (o). However, the electric field in CuMnAs reaches a higher peak value

The same step with a time limitation can be done with the electric field in CuMnAs as follows

$$\begin{aligned} & \max_{\mathbf{q}} \mathbf{q}^H \mathbf{E}^H \mathbf{E} \mathbf{q}, \\ & \text{s.t. } \mathbf{q}^H \mathbf{W} \mathbf{q} = W_0, \\ & \quad \mathbf{q}^H (0.9 \mathbf{U} - \mathbf{U}_T) \mathbf{q} \leq 0, \end{aligned} \quad (11)$$

where \mathbf{U} and \mathbf{U}_T are matrices of the total squared electric field and the squared electric field in the given time interval

for $T = 7\text{ ps}$. The matrices are evaluated equivalently as \mathbf{W} and \mathbf{W}_T except t_d . The electric field at the target point as a function of frequency and unity excitation is taken from CST. The function is multiplied by its complex conjugate image and projected into the set of basis functions ξ_n from Appendix B.

$$\mathbf{U} = \frac{1}{4\pi} \int_{-\infty}^{\infty} a^*(\omega) \mathbf{E}_{\text{CuMnAs}}^H(\omega) \mathbf{E}_{\text{CuMnAs}}(\omega) a(\omega) d\omega. \quad (12)$$

Matrix \mathbf{U}_T differs only by introducing integration over two distinct angular frequencies ω_1, ω_2 and the sinc function in the expression as in (9).

The results are presented in (c) which shows the excitation again spanning a long time, whereas the waveform in CuMnAs outside of the prescribed interval is attenuated compared to the amplitude global maxima which are not far from the optimum without the constraint.

The combination of both constraints for excitation in (b) and for the target field in (c) results in another optimization problem whose solution is presented in (d). Since optimization has more constraints than the previous solutions (a), (b), and (c), performance is lower but still higher than that of the original pulse (o). That shows that optimization has achieved maximum potential in the given scenario considering the constraints. The excitation mostly spans the narrow interval and the electric field in CuMnAs is also mainly accumulated in the given interval. The disparity between (o) and (d) is minimal, so the used design performs almost the best possible. This suggests that enhancement can only be achieved through topological changes even more by co-design of the structure and of the pulse.

The current pulse has already reached its design limits. Thus, achieving better performance necessitates either a re-designed system or a less restricted pulse. This showcases the effectiveness of the tool in configuring pulses for antiferromagnetic memory switching and judging topologies for their capabilities.

V. CONCLUSION

A methodology to determine optimal waveforms is presented in this paper with optimized parameters being defined as linear or quadratic terms. The evaluation requires a post-

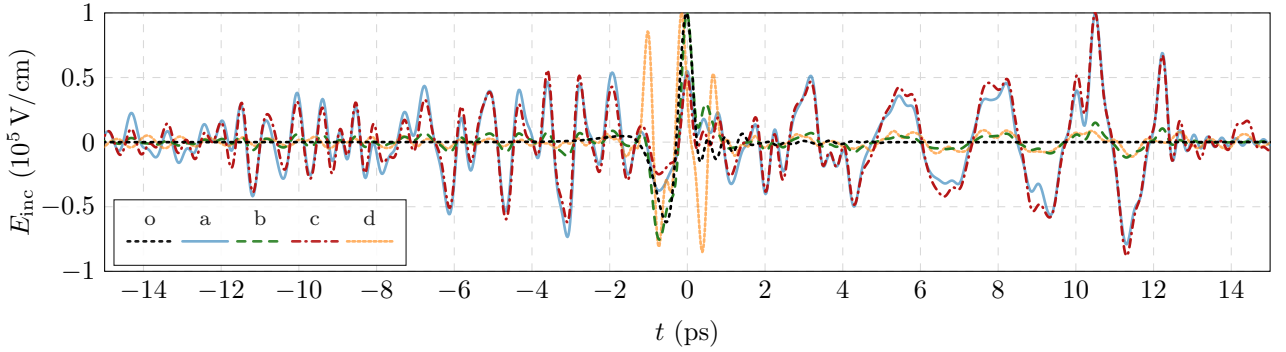


Fig. 15. Incident plane waves at the position of the observation: (o) Pulse used in [45]. (a) Optimal excitation for the maximum peak. (b) Optimal excitation for the maximum peak with a constraint on the incident wave to concentrate 90 % of energy in the 2 ps interval. (c) Optimal excitation for the maximum peak with a constraint in the target field to concentrate 90 % of energy in the 14 ps interval. (d) Optimal excitation for the maximum peak with both constraints in (b) and (c).

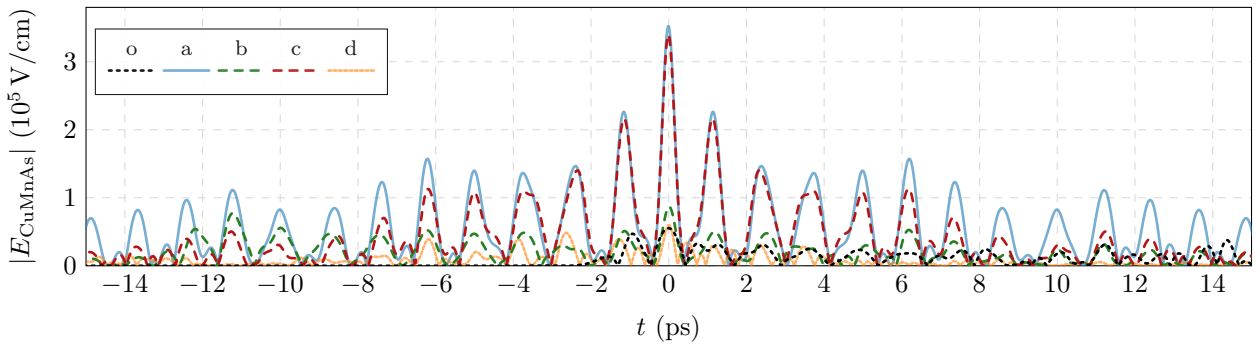


Fig. 16. Magnitude of the electric field in CuMnAs for excitation pulses (o)–(d) in Fig. 15.

processing step based on convex optimization and the input data can be calculated in any EM simulator.

The tool can serve and provide quantitative results in many scenarios, including pulsed radiation or antiferromagnetic memory switching with pulse lasers, as discussed in this paper, as well as the creation of hotspots using near-field energy focusing in lossy materials using antenna arrays for applications such as hyperthermia therapy in medicine.

The capability of the tool is to find the optimal excitation waveform for an arbitrarily chosen target metric. Moreover, the number of sources is not restricted. In the case of an antenna, matching can be omitted. This leads to fundamental bounds based on current density as known in the frequency domain, but now the current, apart from space, can be controlled in time allowing us to evaluate fundamental bounds in the time domain for a given design region based on the current, although the values would in many cases be overly optimistic.

An important strength of the proposed method lies in its practical utility for evaluating and optimizing radiating systems. Given a specific system configuration, the method determines whether the desired pulsed performance can be achieved. If the shape and constraints of the system are sufficient, the method identifies the optimal pulse shape to maximize performance. Conversely, if the system cannot meet the imposed requirements, the approach highlights these limitations, offering valuable insights into whether a redesign of the system geometry is necessary.

By decoupling waveform optimization from structural design, the proposed method ensures a globally optimal solution that can be computed efficiently in polynomial time, unlike the iterative and often local solutions associated with topology optimization. This characteristic guarantees the general applicability of the method to existing antenna systems without necessitating their redesign, while still ensuring the best achievable performance for a given scenario and set of constraints.

While this paper focuses on waveform optimization for a fixed transmitting antenna, the methodology has broader potential. It can be extended to co-design scenarios in which both antenna and waveform design are considered simultaneously, making it applicable to a wider range of advanced engineering problems. In such case, the topology optimization would change the design according to the results computed by the proposed tool, though such a procedure would be computationally intensive. However, this would open the way to the automated design of pulsed radiators, antiferromagnetic memories, or other devices that rely on pulses in the time domain.

APPENDIX A MATRIX OPERATORS FROM EFIE AND MoM

A representative example of an EM solver capable of providing required antenna characteristics is AToM based on EFIE and MoM. The matrix representation of multiple

quantities is presented in [39, Appendix A]. The extraction of essential metrics to the manuscript is presented in this appendix. Multiple ports are considered.

Using EFIE and MoM, the electric field in the far-field zone expressed in the frequency domain reads

$$\mathbf{E}_\infty(\mathbf{r}, \omega) = \mathbf{F}(\mathbf{r}, \omega) \mathbf{I}(\omega) \frac{e^{-j\omega r/c}}{r}, \quad (13)$$

where c is the speed of light, \mathbf{F} is a far-field matrix, and \mathbf{I} is a column vector of current density expansion coefficients.

The essential quantities are far field as a function of the incident waves from the feeding transmission line and their total available energy in (4). The electric far field is computed from far-field matrix \mathbf{F} and current vector \mathbf{I} , see (13). The current is excited by incident waves \mathbf{a} as

$$\mathbf{I}(\omega) = \mathbf{Z}^{-1}(\omega) \mathbf{P} \mathbf{v}(\omega), \quad (14)$$

where \mathbf{Z} is the impedance matrix, and \mathbf{P} is the port matrix which assigns port voltage vector values \mathbf{v} to corresponding positions for the matrix multiplication. Port voltages are given by incident waves as

$$\mathbf{v}(\omega) = \mathbf{k}_i^{-1}(\omega) \mathbf{a}(\omega), \quad (15)$$

with incident waves \mathbf{a} and \mathbf{k}_i interconnecting the lossless feeding transmission lines of characteristic impedance $Z_{\text{char}} = 50 \Omega$ considered in this manuscript with antenna port voltages [46].

Other antenna characteristics can be computed in the same way. Emerging quantities for this application are antenna gain or port reflection coefficients. The study of the characteristics provides information on the suitability of individual antennas for application.

APPENDIX B BAND LIMITED SET OF BASIS FUNCTIONS

This manuscript uses a set of basis functions for the spectral expansion of antenna characteristics. Complex-valued expansion coefficients are denoted as q_n . The functions are band-limited, orthogonal, and continuous, and provide well-behaved real-valued images in iFT. Their explicit form reads

$$\xi_n(\omega) = \frac{1}{\sqrt{\omega_{\max} - \omega_{\min}}} \sin\left(n\pi \frac{|\omega| - \omega_{\min}}{\omega_{\max} - \omega_{\min}}\right) \begin{cases} 1, \\ \text{sign}(\omega)j, \end{cases} \quad (16)$$

where the upper row corresponds to the real part, while the lower row corresponds to the imaginary part. The values ω_{\min} and ω_{\max} define the spectral band interval where the functions are nonzero.

APPENDIX C PROJECTION VIA GALERKIN METHOD

Galerkin method [38], [13] converts continuous operators to matrices using the same basis and testing functions. The method is applied to all operators using functions introduced in Appendix B. The approach is explicitly presented on the

far-field operator and the construction of the far-field power matrix.

The far-filed operator is projected in the following way for optimized time t_{opt}

$$\hat{\mathbf{F}}_{pn}(\mathbf{r}, \omega) = \int_{-\infty}^{\infty} \mathbf{F}(\mathbf{r}, \omega) \mathbf{Z}^{-1}(\omega) \mathbf{P} \mathbf{k}_i^{-1}(\omega) \xi_n(\omega) e^{j\omega t_{\text{opt}}} d\omega, \quad (17)$$

where \mathbf{a}_p excites only the chosen feeding transmission line p by unity amplitude. Here, it is presented for operators from MoM, see Appendix A, but the same methodology can be applied to antenna characteristics from an arbitrary EM solver. The far-field operator projected has two rows corresponding to polarizations and pn columns with a linear index that combines ports and basis functions. The far-filed operator allows us to define the far-field power matrix

$$\mathbf{S}(\mathbf{r}, \omega) = \hat{\mathbf{F}}^H(\mathbf{r}, \omega) \hat{\mathbf{F}}(\mathbf{r}, \omega) \quad (18)$$

in (8).

REFERENCES

- [1] R. McIntosh and J. Sarna, "Bounds on the optimum performance of planar antennas for pulse radiation," *IEEE Transactions on Antennas and Propagation*, vol. 30, no. 3, pp. 381–389, 1982.
- [2] Y. Kang and D. Pozar, "Optimization of pulse radiation from dipole arrays for maximum energy in a specified time interval," *IEEE Transactions on Antennas and Propagation*, vol. 34, no. 12, pp. 1383–1390, 1986.
- [3] D. Hackett, C. Taylor, D. McLemore, H. Dogliani, W. Walton, and A. Leyendecker, "A transient array to increase the peak power delivered to a localized region in space: part I-theory and modeling," *IEEE Transactions on Antennas and Propagation*, vol. 50, no. 12, pp. 1743–1750, Dec. 2002.
- [4] J. Maloney and G. Smith, "Optimization of a conical antenna for pulse radiation: an efficient design using resistive loading," *IEEE Transactions on Antennas and Propagation*, vol. 41, no. 7, pp. 940–947, Jul. 1993.
- [5] Y. Yang and A. Fathy, "See-through-wall imaging using ultra wideband short-pulse radar system," in *2005 IEEE Antennas and Propagation Society International Symposium*, ser. APS-05. IEEE, 2005.
- [6] Z. Chen, M. Foegelle, and T. Harrington, "Analysis of log periodic dipole array antennas for site validation and radiated emissions testing," in *1999 IEEE International Symposium on Electromagnetic Compatibility. Symposium Record (Cat. No.99CH36261)*, ser. ISEMCA-99. IEEE, 1999.
- [7] D. Pozar, R. McIntosh, and S. Walker, "The optimum feed voltage for a dipole antenna for pulse radiation," *IEEE Transactions on Antennas and Propagation*, vol. 31, no. 4, pp. 563–569, 1983.
- [8] D. Pozar, D. Schaubert, and R. McIntosh, "The optimum transient radiation from an arbitrary antenna," *IEEE Transactions on Antennas and Propagation*, vol. 32, no. 6, pp. 633–640, 1984.
- [9] D. Pozar, Y. Kang, D. Schaubert, and R. McIntosh, "Optimization of the transient radiation from a dipole array," *IEEE Transactions on Antennas and Propagation*, vol. 33, no. 1, pp. 69–75, 1985.
- [10] M. Onder and M. Kuzuoglu, "Optimal control of the feed voltage of a dipole antenna," *IEEE Transactions on Antennas and Propagation*, vol. 40, no. 4, pp. 414–421, Apr. 1992.
- [11] P. van Etten, "The present technology of impulse radars," in *Radar-77*, Jan. 1977, pp. 535–539. [Online]. Available: <https://ui.adsabs.harvard.edu/abs/1977rpi..conf..535V>
- [12] W. C. Chew, M. S. Tong, and B. Hu, *Integral Equation Methods for Electromagnetic and Elastic Waves*. Morgan & Claypool, 2009.
- [13] R. F. Harrington, *Field Computation by Moment Methods*. Piscataway, New Jersey, United States: Wiley – IEEE Press, 1993.
- [14] S. Boyd and L. Vandenberghe, *Convex Optimization*. Cambridge, Great Britain: Cambridge University Press, 2004.
- [15] M. Gustafsson, M. Capek, and K. Schab, "Tradeoff between antenna efficiency and Q-factor," *IEEE Trans. Antennas Propag.*, vol. 67, no. 4, pp. 2482–2493, Apr. 2019.

[16] M. Gustafsson and M. Capek, "Maximum gain, effective area, and directivity," *IEEE Trans. Antennas Propag.*, vol. 67, no. 8, pp. 5282–5293, Aug. 2019.

[17] M. Gustafsson, D. Tayli, C. Ehrenborg, M. Cismasu, and S. Norbedo, "Antenna current optimization using MATLAB and CVX," *FERMAT*, vol. 15, no. 5, pp. 1–29, May–June 2016. [Online]. Available: https://efermat.github.io/articles/Gustafsson-ART-2016-Vol15-May_Jun-005/

[18] P. Chao, B. Strekha, R. Kuate Defo, S. Molesky, and A. W. Rodriguez, "Physical limits in electromagnetism," *Nature Reviews Physics*, vol. 4, no. 8, pp. 543–559, Jul. 2022.

[19] J. Liska, L. Jelinek, and M. Capek, "Computation of fundamental bounds for antennas," in *2022 16th European Conference on Antennas and Propagation (EuCAP)*. IEEE, Mar. 2022.

[20] J. Liska, M. Gao, L. Jelinek, E. R. Algar, A. K. Skrivelik, and M. Capek, "Upper bound on implantable antennas considering ohmic loss," *IEEE Transactions on Antennas and Propagation*, vol. 72, no. 4, pp. 3507–3516, Apr. 2023.

[21] L. Jelinek, M. Gustafsson, M. Capek, and K. Schab, "Fundamental bounds on the performance of monochromatic passive cloaks," *Optics Express*, vol. 29, no. 15, pp. 24 068–24 082, 2021.

[22] P. S. Venkataram, S. Molesky, W. Jin, and A. W. Rodriguez, "Fundamental limits to radiative heat transfer: The limited role of nanostructuring in the near-field," *Phys. Rev. Lett.*, vol. 124, p. 013904, Jan 2020. [Online]. Available: <https://link.aps.org/doi/10.1103/PhysRevLett.124.013904>

[23] J. Liska, L. Jelinek, and M. Capek, "Performance bounds of magnetic traps for neutral particles," *Physical Review A*, vol. 106, no. 5, p. 053110, Nov. 2022.

[24] J. Mohajan, P. Chao, W. Jin, S. Molesky, and A. W. Rodriguez, "Fundamental limits on χ^2 second harmonic generation," *arXiv*, 2023.

[25] V. G. Polevoi, "Maximum energy extractable from an electromagnetic field," *Radiophysics and Quantum Electronics*, vol. 33, no. 7, pp. 603–609, 1990.

[26] L. Jelinek, J. Liska, and M. Capek, "Upper bound on instantaneous power flux," in *2023 IEEE International Symposium on Antennas and Propagation and USNC-URSI Radio Science Meeting (USNC-URSI)*. IEEE, Jul. 2023.

[27] J. Nocedal and S. Wright, *Numerical Optimization*. New York, United States: Springer, 2006.

[28] J. Liska, L. Jelinek, and M. Capek, "Maximum peak radiation intensity," in *2023 24th International Conference on Applied Electromagnetics and Communications (ICECOM)*. IEEE, Sep. 2023.

[29] X.-K. Wang, L. Tian, H.-L. Wang, and X.-W. Zhu, "Design of an ultra-wideband picosecond pulse generator based on step recovery diodes with an improved SPICE model," *International Journal of Circuit Theory and Applications*, vol. 51, no. 8, pp. 3585–3595, Mar. 2023.

[30] W. L. Stutzman and G. A. Thiele, *Antenna theory and design*. John Wiley & Sons, 2012.

[31] D. M. Pozar, "Optimal radiated waveforms from an arbitrary UWB antenna," *IEEE Transactions on Antennas and Propagation*, vol. 55, no. 12, pp. 3384–3390, Dec. 2007.

[32] R. F. Harrington, "Effect of antenna size on gain, bandwidth, and efficiency," *J. Res. Nat. Bur. Stand.*, vol. 64-D, pp. 1–12, Jan.–Feb. 1960.

[33] K. Shlager, G. Smith, and J. Maloney, "Optimization of bow-tie antennas for pulse radiation," *IEEE Transactions on Antennas and Propagation*, vol. 42, no. 7, pp. 975–982, Jul. 1994.

[34] J.-H. Wang, L. Jen, and S.-S. Jian, "Optimization of the dipole shapes for maximum peak values of the radiating pulse," in *IEEE Antennas and Propagation Society International Symposium 1997. Digest*, ser. APS-97. IEEE, 1997.

[35] D. Pozar, "Waveform optimizations for ultrawideband radio systems," *IEEE Transactions on Antennas and Propagation*, vol. 51, no. 9, pp. 2335–2345, Sep. 2003.

[36] T. Liang and Y.-Z. Xie, "Waveform shaping for maximizing the sharpness of receiving voltage waveform for an ultra-wideband antenna system," *IEEE Transactions on Antennas and Propagation*, vol. 69, no. 9, pp. 5924–5930, Sep. 2021.

[37] (2022) CST Computer Simulation Technology. Dassault Systemes. [Online]. Available: <https://www.3ds.com/products-services/simulia-products/cst-studio-suite/>

[38] L. V. Kantorovich and G. P. Akilov, *Functional analysis*. Oxford New York: Pergamon Press, 1982.

[39] J. Liska, L. Jelinek, and M. Capek, "Fundamental bounds to time-harmonic quadratic metrics in electromagnetism: Overview and implementation," *arXiv*, 2021. [Online]. Available: <https://arxiv.org/abs/2110.05312>

[40] (2024) Antenna Toolbox for MATLAB (AToM). Czech Technical University in Prague. www.antennatoolbox.com. [Online]. Available: www.antennatoolbox.com

[41] B. Gustavsen and A. Semlyen, "Rational approximation of frequency domain responses by vector fitting," *IEEE Trans. Power Delivery*, vol. 14, pp. 1052–1061, 1999.

[42] J. Yang and A. Kishk, "A novel low-profile compact directional ultra-wideband antenna: The self-grounded bow-tie antenna," *IEEE Transactions on Antennas and Propagation*, vol. 60, no. 3, pp. 1214–1220, Mar. 2012.

[43] T. Hertel and G. Smith, "The conical spiral antenna over the ground," *IEEE Transactions on Antennas and Propagation*, vol. 50, no. 12, pp. 1668–1675, Dec. 2002.

[44] C. A. Balanis, *Advanced Engineering Electromagnetics*. Hoboken, NJ: Wiley, 1989.

[45] K. Olejník, T. Seifert, Z. Kašpar, V. Novák, P. Wadley, R. P. Campion, M. Baumgartner, P. Gambardella, P. Němec, J. Wunderlich, J. Sinova, P. Kužel, M. Müller, T. Kampfrath, and T. Jungwirth, "Terahertz electrical writing speed in an antiferromagnetic memory," *Science Advances*, vol. 4, no. 3, Mar. 2018.

[46] M. Capek, L. Jelinek, and M. Masek, "Finding optimal total active reflection coefficient and realized gain for multi-port lossy antennas," *IEEE Trans. Antennas Propag.*, vol. 69, no. 5, pp. 2481–2493, Oct. 2021.



Jakub Liska received his B.Sc. and M.Sc. degrees in electrical engineering from the Czech Technical University in Prague, Czech Republic, in 2019 and 2021, respectively. He is currently pursuing a Ph.D. in electrical engineering at the same university.

His research interests include EM field theory, fundamental bounds, computational electromagnetics, numerical and convex optimization, numerical techniques, and eigenproblems.



Lukas Jelinek was born in Czech Republic in 1980. He received his Ph.D. degree from the Czech Technical University in Prague, Czech Republic, in 2006. In 2015 he was appointed Associate Professor at the Department of Electromagnetic Field at the same university.

His research interests include wave propagation in complex media, electromagnetic field theory, metamaterials, numerical techniques, and optimization.



Miloslav Capek (M'14, SM'17) received the M.Sc. degree in Electrical Engineering 2009, the Ph.D. degree in 2014, and was appointed a Full Professor in 2023, all from the Czech Technical University in Prague, Czech Republic.

He leads the development of the AToM (Antenna Toolbox for Matlab) package. His research interests include electromagnetic theory, electrically small antennas, antenna design, numerical techniques, and optimization. He authored or co-authored over 165 journal and conference papers.

Dr. Capek is the Associate Editor of IET Microwaves, Antennas & Propagation. He was a regional delegate of EurAAP between 2015 and 2020 and an associate editor of Radioengineering between 2015 and 2018. He received the IEEE Antennas and Propagation Edward E. Alshuler Prize Paper Award 2022 and ESoA (European School of Antennas) Best Teacher Award in 2023.